

Clinkering-free cementation by fly ash carbonation

Zhenhua Wei^a, Bu Wang^a, Gabriel Falzone^{a,b}, Erika Callagon La Plante^a,
Monday Uchenna Okoronkwo^a, Zhenyu She^c, Tandre Oey^a, Magdalena Balonis^{b,d},
Narayanan Neithalath^e, Laurent Pilon^c, Gaurav Sant^{a,b,f,*}

^a Laboratory for the Chemistry of Construction Materials (LC²), Department of Civil and Environmental Engineering, University of California, Los Angeles, CA 90095, USA

^b Department of Materials Science and Engineering, University of California, Los Angeles, CA 90095, USA

^c Department of Mechanical and Aerospace Engineering, University of California, Los Angeles, CA 90095, USA

^d Institute for Technology Advancement, University of California, Los Angeles, CA 90095, USA

^e School of Sustainable Engineering and the Built-Environment, Arizona State University, Tempe, AZ 85287, USA

^f California Nanosystems Institute (CNSI), University of California, Los Angeles, CA 90095, USA



ARTICLE INFO

Keywords:

Fly ash
Cementation
CO₂
Upcycling
Strength
Concrete

ABSTRACT

The production of ordinary portland cement (OPC) is a CO₂ intensive process. Specifically, OPC clinkering reactions not only require substantial energy in the form of heat, but they also result in the release of CO₂; i.e., from both the decarbonation of limestone and the combustion of fuel to provide heat. To create alternatives to this CO₂ intensive process, this paper demonstrates a new route for clinkering-free cementation by the carbonation of fly ash; i.e., a by-product of coal combustion. It is shown that in moist environments and at sub-boiling temperatures, Ca-rich fly ashes react readily with gas-phase CO₂ to produce robustly cemented solids. After seven days of exposure to vapor-phase CO₂ at 75 °C, such formulations achieve a compressive strength of around 35 MPa and take-up 9% CO₂ (i.e., by mass of fly ash solids). On the other hand, Ca-poor fly ashes due to their reduced alkalinity (i.e., low abundance of mobile Ca- or Mg-species), show limited potential for CO₂ uptake and strength gain—although this deficiency can be somewhat addressed by the provision of supplemental/extrinsic Ca agents. The roles of CO₂ concentration and processing temperature are discussed, and linked to the progress of reactions and the development of microstructure. The outcomes create new pathways for achieving clinkering-free cementation while enabling the beneficial utilization (“upcycling”) of emitted CO₂ and fly ash; i.e., two abundant, but underutilized industrial by-products.

1. Introduction and background

Over the last century, for reasons of its low-cost and the widespread geographical abundance of its raw materials, ordinary portland cement (OPC) concrete has been used as the primary material for the construction of buildings and other infrastructure [1–3]. However, the production of OPC is a highly energy- and CO₂-intensive process. For example, at a production level of 4.2 billion tons annually [4] (equivalent to > 30 billion tons of concrete produced [5]), OPC production accounts for approximately 3% of primary energy use and results in nearly 9% of anthropogenic CO₂ emissions, globally [2]. Such CO₂ release is attributed to factors including: (i) the combustion of fuel required for clinkering the raw materials (i.e., limestone and clay) at 1450 °C [6,7], and, (ii) the release of CO₂ during the calcination of limestone in the cement kiln [2,7]. As a result, around 0.9 tons of CO₂

are emitted per ton of OPC produced [8]. Therefore, there is great need to reduce the CO₂ footprint of cement, and secure alternative solutions for ‘cementation’ as required for building and infrastructure construction.

Furthermore, there exist unique challenges associated with the production of electricity using coal (or natural gas) as the fuel source. For example, coal power is not only associated with significant CO₂ emissions (i.e., 30% of anthropogenic CO₂ emissions worldwide [9]), but also results in the accumulation of significant quantities of solid wastes such as fly ash (600 million tons annually worldwide [10]). While considerable efforts have been made to replace OPC in the binder fraction of concrete by supplementary cementitious materials (SCMs) such as fly ash, the extent of such utilization remains limited. For example, in the U.S., only around 45% of all fly ash produced annually is beneficially utilized to partially replace in the concrete [11]. In spite of

* Corresponding author at: Laboratory for the Chemistry of Construction Materials (LC²), Department of Civil and Environmental Engineering, University of California, Los Angeles, CA 90095, USA.

E-mail address: gsant@ucla.edu (G. Sant).

<https://doi.org/10.1016/j.jcou.2017.11.005>

Received 18 September 2017; Received in revised form 2 November 2017; Accepted 17 November 2017
2212-9820/ © 2017 Elsevier Ltd. All rights reserved.

supportive frameworks [12], such limited use is due to factors including: (i) the presence of impurities including air-pollution control (APC) residues and unburnt carbon as a result of which some fly ashes are non-compliant (e.g., as per ASTM C618 [13]) for use in traditional OPC concrete, due to durability concerns [14,15], and, (ii) increasing cement replacement (i.e., fly ash dosage) levels to greater than 25 mass % is often associated with extended setting times and slow strength gain resulting in reduced constructability of the concrete [14,16].

Clearly, there is an immediate need to valorize or beneficially utilize (“upcycle”) vapor and solid wastes associated with coal power production. However, given the tremendous scale of waste production, there is a need to secure upcycling opportunities of some prominence; e.g., within the construction sector wherein large-scale utilization of upcycled materials can be achieved. This condition could be satisfied if the “upcycled solution” is able to serve as an alternative to OPC (and OPC-concrete) so long as it is able to fulfill the functional and performance requirements of construction. Mineral carbonation (i.e., conversion of vapor phase CO₂ into a carbonaceous mineral, e.g., CaCO₃) has been proposed as a promising route to sequester CO₂ in alkaline solids [17–19]. In such a process, CO₂ is sequestered by the chemical reaction of CO₂ streams with light-metal oxides to form thermodynamically stable carbonates; thus enabling permanent and safe storage of CO₂ [19]. While numerous studies have examined different alkaline waste streams to render cementation solutions—for example, coal combustion residues [20], municipal incinerator wastes [21], and wastes from iron and steel production [22,23]—the low production throughput, or severe operating conditions (i.e., high temperature and elevated CO₂ pressure) [7,21,24,25] have made typical approaches difficult to implement at a practical scale [17]. As such, in this study, two abundant by-products secured from coal-fired power plants (i.e., fly ash and CO₂ borne in flue gas) are utilized to demonstrate a route towards achieving cementation, by the carbonation of fly ash and without any need for clinkering (i.e., the traditional high temperature process of OPC production). It is shown that Ca-rich fly ashes react readily with CO₂ under moist conditions, at atmospheric pressure and at sub-boiling temperatures. The influences of Ca availability in the fly ash, CO₂ concentration, and processing temperature on reaction kinetics and strength gain are discussed. Taken together, the outcomes of this study create new opportunities for the simultaneous valorization of solid wastes and flue gas borne CO₂, within an integrated process.

2. Materials and methods

2.1. Materials

Class C (Ca-rich) and Class F (Ca-poor) fly ashes compliant with ASTM C618 [13] were used. An ASTM C150 [26] compliant Type I/II ordinary portland cement (OPC) was used as a cementation reference. The bulk oxide compositions of the fly ashes and OPC as determined by X-ray fluorescence (XRF) are shown in Table 1. The crystalline compositions of the Ca-rich and Ca-poor fly ashes as determined using X-ray diffraction (XRD) are shown in Table 2. It should be noted that these two fly ashes were used since they represent typical Ca-rich and Ca-poor variants in the U.S., and since Ca content is expected to strongly influence the extent of CO₂ uptake and strength development of carbonated fly ash formulations.

2.2. Experimental methods

2.2.1. Particle size distribution and specific surface area

The particle size distribution (PSD) of OPC was measured using static light scattering (SLS) using a Beckman Coulter LS13-320 particle sizing apparatus fitted with a 750 nm light source. The solid was dispersed into primary particles via ultrasonication in isopropanol (IPA), which was also used as the carrier fluid. The complex refractive index of OPC was taken as $1.70 + 0.10i$ [28]. The uncertainty in the PSD was

Table 1

The simple oxide composition of the fly ashes and OPC as determined using X-ray fluorescence (XRF) [27].

Simple Oxide	Mass (%)		
	Ca-rich Fly Ash	Ca-poor Fly Ash	Type I/II OPC
SiO ₂	35.44	53.97	20.57
Al ₂ O ₃	17.40	20.45	5.19
Fe ₂ O ₃	7.15	5.62	3.44
SO ₃	2.34	0.52	2.63
CaO	26.45	12.71	65.99
Na ₂ O	1.90	0.57	0.17
MgO	5.73	2.84	1.37
K ₂ O	0.53	1.11	0.31
P ₂ O ₅	0.95	0.30	0.08
TiO ₂	1.19	1.29	0.26
Density (kg/m ³)	2760	2470	3150
Specific surface area (SSA, m ² /kg) ^a	4292.6	616.8	442.6

^a The surface area of the Ca-rich (Class C) fly ash is significantly overestimated by N₂ adsorption due to the presence of unburnt carbon [27]. However, based on kinetic analysis of reaction rates in OPC + fly ash + water systems, it can be inferred that the reactive surface areas of both the Ca-rich and Ca-poor fly ashes are similar to each other, and that of OPC. Further discussion regarding the surface areas of these materials can be found elsewhere [27].

Table 2

The mineralogical composition of the fly ashes and OPC as determined using quantitative X-ray diffraction (XRD) and Rietveld refinement [27].

Composition	Mass %		
	Ca-rich Fly Ash	Ca-poor Fly Ash	Type I/II OPC
Lime (CaO)	1.16	–	0.5
Periclase (MgO)	3.81	0.30	–
Quartz (SiO ₂)	10.06	16.64	–
Calcite (CaCO ₃)	0	0	4.60
Mullite (Al ₆ Si ₂ O ₁₃)	0.86	5.08	–
Anhydrite (CaSO ₄)	2.80	0.97	1.2
Gypsum (CaSO ₄ ·2H ₂ O)	–	–	1.1
Magnetite (Fe ₃ O ₄)	1.66	1.76	–
Merwinite (Ca ₃ Mg(SiO ₄) ₂)	6.98	–	–
Gehlenite (Ca ₂ Al ₂ SiO ₇)	4.45	–	–
Ca ₂ SiO ₄ (C ₂ S)	4.93	–	18.00
Ca ₄ Al ₂ Fe ₂ O ₁₀ (C ₄ AF)	–	–	11.40
Ca ₃ Al ₂ O ₆ (C ₃ A)	8.03	–	6.30
Ca ₃ SiO ₅ (C ₃ S)	–	–	56.50
Amorphous	55.26	75.25	–

around 6% based on six replicate measurements. From the PSD, the specific surface area (SSA, units of m²/kg) of OPC was calculated by factoring in its density of 3150 kg/m³, whereas the SSAs of the fly ashes were determined by N₂-BET measurements, as previously reported (see Table 1) [27].

2.2.2. Carbonation processing

Cementitious formulations are processed in the form of slurries, i.e., mixtures of solids (discrete particles) in water (continuous phase) [14]. To maintain consistency with established methods of processing cementing materials, slurries of fly ash in deionized (DI) water (i.e., fly ash pastes) were formulated using a planetary mixer at a water-to-solids mass ratio of 0.20 (w/s = 0.20). The fly ash pastes offered sufficient fluidity such that they could be poured—following ASTM C192 [29]. The pastes were then cast into molds to prepare cubic specimens with a dimension of 50 mm on each side. Following 2 h of curing in the molds at temperature, T = 45 ± 0.2 °C and relative humidity, RH = 50 ± 1%, the specimens were demolded after which on account of evaporation they featured a reduced water content, i.e., w/s = 0.15, but were able to hold form; that is, they were “shape stabilized”. At this

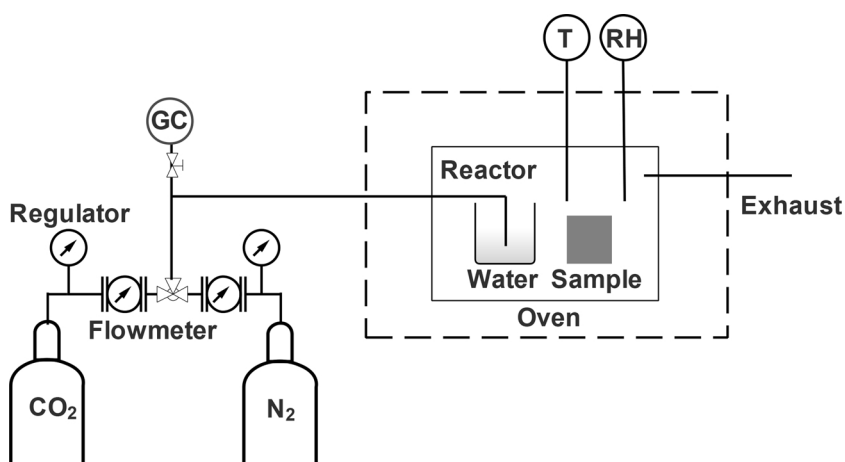


Fig. 1. A schematic of the carbonation reactor showing the vapor streams, sample placement, and monitoring and control units (e.g., flow-meters, pressure regulators, temperature/relative humidity [T/RH] meters, and gas chromatograph (GC)).

time, the cubes were placed in a carbonation reactor, a schematic of which is shown in Fig. 1.

Gas-phase CO₂ at atmospheric pressure with a purity of 99.5% (“pure CO₂”) was used for carbonation. On the other hand, 99% pure N₂ at atmospheric pressure was used as a control vapor that simulated ambient air (i.e., with a CO₂ abundance of around 400 ppm [30]). In addition, a simulated flue gas was created by mixing the pure N₂ and pure CO₂ streams to yield a vapor with 12% CO₂ (v/v) as confirmed using an Inficon F0818 gas chromatography (GC) instrument. Prior to contacting the samples, all gas streams were bubbled into an open, water-filled container to produce a condensing environment in the reactor (i.e., as shown in Fig. 1). Each of the vapors were contacted with the cubical samples at temperatures of 45 ± 0.2 °C, 60 ± 0.2 °C, and 75 ± 0.2 °C.

2.2.3. Compressive strength

The compressive strengths of the fly ash cubes (i.e., both control samples, and those exposed to CO₂) were measured at 1 day intervals following ASTM C109 [31] for up to 10 days. All strength data reported herein are the average of three replicate specimens cast from the same mixing batch. For comparison, the compressive strengths of neat OPC pastes prepared at w/s = 0.30, 0.40, 0.50, and 0.60 were measured after 1, 3, 7, and 28 days of immersion and curing in a Ca(OH)₂-saturated solution (“limewater”) at 23 ± 2 °C.

2.2.4. CO₂ uptake by fly ash formulations

CO₂ uptake due to carbonation of the fly ashes was quantified by two methods: (i) a mass-gain method, and, (ii) thermogravimetric analysis (TGA). The mass-gain method was used to estimate the average CO₂ uptake of the bulk cubic specimen from the mass gain of three replicate cubes following CO₂ contact as given by Eq. (1),

$$w = \frac{m_t - m_i}{m_a} \quad (1)$$

where, w (g/g) is the CO₂ uptake of a given cube, m_t (g) is the mass of the specimen following CO₂ contact over a period of time t (days), m_i (g) is the initial mass of the specimen, and m_a (g) is the mass of dry fly ash contained in the specimen (i.e., estimated from the mixture proportions). It should be noted that carbonation is an exothermic reaction; thus it could result in the evaporation of water from the sample. However, since herein, curing was carried out in a near-condensing atmosphere, mass measurements before and after carbonation revealed no mass loss due to (moisture) evaporation. The ratio of CO₂ uptake at time t to that assessed at the end of the experiment (i.e., CO₂ uptake fraction, α) is given by Eq. (2),

$$\alpha = \frac{m_t - m_i}{m_f - m_i} \quad (2)$$

where, m_f (g) is the final mass of a given cubical specimen following 10 days of CO₂ exposure.

TGA was used to determine the extent of CO₂ uptake at different depths in the fly ash cubes, from the surface to the center in 5 mm increments. To accomplish so, cubes were sectioned longitudinally using a hand saw. Then, samples were taken from the newly exposed surface along a mid-line using a drill at a sampling resolution of around ± 1 mm. The dust and debris obtained during drilling, at defined locations along the center-line, were collected and pulverized for thermal analysis in a PerkinElmer STA 6000 simultaneous thermal analyzer (TGA/DTG/DTA) provided with a Pyris data acquisition interface. Herein, ≈ 30 mg of the powdered sample that passed a 53 μm sieve was heated under ultra-high purity (UHP)-N₂ gas purged at a flow rate of 20 mL/min and heating rate of 10 °C/min in pure aluminum oxide crucibles over a temperature range of 35-to-980 °C. The mass loss (TG) and differential weight loss (DTG) patterns acquired were used to quantify the CO₂ uptake by assessing the mass loss associated with calcium carbonate decomposition in the temperature range 550 °C ≤ T ≤ 900 °C [7]. It should be noted that because our quantifications of CO₂ uptake are based on the amount of CO₂ sequestered in the solid phase (i.e., in the form of CaCO₃), a correction for the amount of CO₂ dissolved in water (i.e., CO_{2(aq)}), as determined by Henry’s law [32], and the species CO₃²⁻ and HCO₃⁻ is not needed. The mass-based method of assessing the extent of carbonation and the spatially resolved TGA method indicate, on average, similar levels of carbonation, as noted below.

2.2.5. X-ray diffraction (XRD)

To qualitatively examine the effects of carbonation, the mineralogical compositions of fly ash mixtures before and after CO₂ exposure were assessed using XRD. Here, entire fly ash cubes were crushed and ground into fine powders, and XRD patterns were collected by scanning from 5-to-70° (2θ) using a Bruker-D8 Advance diffractometer in a θ-θ configuration with Cu-Kα radiation (λ = 1.54 Å) fitted with a VANTEC-1 detector. Representative powder samples were examined to obtain averaged data over the whole cube. The diffractometer was run in continuous mode with an integrated step scan of 0.021° (2θ). A fixed divergence slit of 1.00° was used during X-ray data acquisition. To minimize artifacts resulting from preferred orientation and to acquire statistically relevant data, the (powder) sample surface was slightly textured and a rotating sample stage was used.

2.2.6. Scanning electron microscopy (SEM)

The morphology and microstructure of the uncarbonated and carbonated fly ash mixtures were examined using a field emission scanning electron microscope provisioned with an energy dispersive X-ray

spectroscopy detector (SEM-EDS; FEI NanoSEM 230). First, hardened samples were sectioned using a hand saw. Then, these freshly exposed sections were taped onto a conductive carbon adhesive and then gold-coated to facilitate electron conduction and minimize charge accumulation on the (otherwise) non-conducting surfaces [28]. Secondary electron (SE) images were acquired at an accelerating voltage of 10 kV and a beam current of 80 pA.

2.3. Thermodynamic simulations of phase equilibria and CO₂ uptake

To better understand the effects of carbonation on the mineralogy and mechanical property development of carbonated fly ashes, thermodynamic calculations were carried out using GEM-Selektor, version 2.3 (GEMS, see Kulik et al. [33,34]). GEMS is a broad-purpose geochemical modeling code which uses Gibbs energy minimization criteria to compute equilibrium phase assemblages and ionic speciation in a complex chemical system from its total bulk elemental composition. Chemical interactions involving solid phases, solid solutions, and the aqueous electrolyte(s) are considered simultaneously. The thermodynamic properties of all the solid and the aqueous species were sourced from the GEMS-PSI database [35–37], with additional data for the cement hydrates sourced from elsewhere [38–40]. The Truesdell-Jones modification of the extended Debye-Hückel equation (see Eq. (3)) [41] was used to account for the effects of solution non-ideality:

$$\log \gamma_j = \frac{-Az_j^2 \sqrt{I}}{1 + B\alpha_j \sqrt{I}} + bI + \log_{10} \frac{x_{jw}}{X_w} \quad (3)$$

where, γ_j is the activity coefficient of j^{th} ion (unitless); z_j is the charge of j^{th} ion, α_j is the ion-size parameter (i.e., effective hydrated diameter of j^{th} ion, Å), A ($\text{kg}^{1/2} \cdot \text{mol}^{-1/2}$) and B ($\text{kg}^{1/2} \cdot \text{mol}^{-1/2} \cdot \text{m}^{-1}$) are pressure, p - and T -dependent Debye-Hückel electrostatic parameters [37], b is a semi-empirical parameter that describes short-range interactions between charged aqueous species in an electrolyte, I is the molal ionic strength of the solution (mol/kg), x_{jw} is the molar quantity of water, and X_w is the total molar amount of the aqueous phase. It should be noted that this solution phase model is suitable for $I \leq 2.0$ mol/kg beyond which, its accuracy is reduced [33]. In the simulations, Ca-rich and Ca-poor fly ashes were reacted with water in the presence of a vapor phase consisting of: (a) air (≈ 400 ppm CO₂), (b) 12% CO₂ (88% N₂, v/v), and, (c) 100% CO₂ (v/v). The calculations were carried out at $T = 75$ °C and $p = 1$ bar. The solid phase distribution was calculated as a function of degree of reaction of the fly ash, until either the pore solution is exhausted (i.e., constraints on water availability) or the fly ash is fully reacted.

3. Results and discussion

3.1. Carbonation strengthening

Fig. 2(a) shows the compressive strength development as a function of time for Class C (Ca-rich) and Class F (Ca-poor) fly ash pastes carbonated in pure CO₂ at 75 °C. The Ca-rich fly ash formulations show rapid strength gain following exposure to CO₂, particularly during the first 6 days. For example, after only 3 days of CO₂ exposure, the carbonated formulation achieves a strength of 25 MPa, whereas a strength on the order of 35 MPa is produced after 7 days of CO₂ exposure. On the other hand, as also seen in Fig. 2(a), when the Ca-rich formulation was exposed to N₂ at the same T , RH , and gas flow rate (i.e., serving as a “control” system), a strength of only 15 MPa develops after 7 days, due to limited reaction of readily soluble Ca-compounds with any available silica, water, and ambient CO₂. As such, the level of strength developed in the control system is less than half of that in the carbonated (Ca-rich) fly ash formulation. The extent of strength development that is noted in the carbonated system is significant as it suggests that carbonated

binders can fulfill code-based (strength) criteria relevant to structural construction¹ (i.e., ≥ 30 MPa as per ACI 318 [43]).

To provide a point of reference, the compressive strengths of neat-OPC formulations were measured across a range of w/s . For example, Fig. 2(b) shows that the compressive strength of a Ca-rich fly ash formulation following exposure to CO₂ for 7 days at 75 °C—around 35 MPa—is equivalent to that of an OPC formulation prepared at $w/s \approx 0.50$ and cured in limewater at 23 °C over the same time period. It is important to note, however, that the fly ash formulations show a significantly reduced rate of strength gain after 7 days—likely due to the consumption of readily available species (Ca, Mg) that can form carbonate compounds. On the other hand, OPC systems show a strength increase on the order of 30% from 7 days to 28 days (i.e., a common aging period that is noted in building codes [43]) of maturation across all w/s .

Furthermore, Fig. 2(a) also indicates that, unlike the “carbonation strengthening” seen in Ca-rich fly ash formulations, Ca-poor fly ash systems showed a strength of ≤ 7 MPa even after 10 days of carbonation, a gain of only ≤ 2 MPa following CO₂ exposure vis-à-vis a system cured in a N₂ atmosphere. This suggests that, in general, Ca-poor fly ashes feature little potential for CO₂ mineralization or strength gain following CO₂ exposure because the amount of Ca and Mg available therein is either insufficient or not easily available for reaction (e.g., see Table 1, Fig. 4). This suggests that carbonation strengthening is dominantly on account of the presence of reactive, alkaline compounds, i.e., Ca- and Mg-bearing compounds (e.g., CaO, MgO, etc.), and Ca present in the fly ash glass (see Tables 1 and 2), that can react with CO₂. It should also be noted that unlike the Ca-poor fly ash, the Ca-rich fly ash contains cementitious phases such as Ca₂SiO₄, Ca₂Al₂SiO₇, and Ca₃Al₂O₆ (see Table 2), which upon hydration (and carbonation) form cementitious compounds such as the calcium-silicate-hydrates (C-S-H), or in a CO₂ enriched atmosphere, calcite and hydrous silica (e.g., see Figs. 3 and 4). As a result, when such Ca-rich fly ash reacts with CO₂ in a moist, super-ambient (i.e., but sub-boiling) environment, carbonate compounds such as calcite (CaCO₃) and magnesite (MgCO₃) are formed as shown in Figs. 3 and 4. This is not observed in the Ca-poor fly ash due to both its much lower total Ca and Mg content and their lower reactivity [27,44] (e.g., see Figs. 3 and 4, which shows little if any formation of carbonate minerals following CO₂ exposure). It should be noted that while the extents of reaction of the fly ashes (i.e., Ca-rich or Ca-poor) were not explicitly assessed, it is expected that their degree of reaction is $\leq 25\%$ for the short reaction times and over the temperature conditions of relevance to this study [45].

In general, upon contact with water, the reactive crystalline (e.g., CaO, Ca₃Al₂O₆, etc.) and amorphous compounds present in a Ca-rich fly ash are expected to rapidly dissolve in the first few minutes. As the pH systematically increases, with continuing dissolution, alkaline species including Na, K, Ca are expected to be released progressively from the glassy compounds [46]. This is expected to result in the development of a silica-rich rim on the surfaces of fly ash particles [47]. Pending the presence of sufficient solubilized Ca, and in the presence of dissolved CO₂, calcite is expected to form rapidly on the surfaces of leached (and other) particles, thereby helping proximate particles to adhere to each other as the mechanism of carbonation strengthening [10,20,48] (e.g., see Figs. 3–5). This is additionally helped by the liberation of Ca-, and Si- from the anhydrous fly ash, whose reaction with water results in the formation of hydrated calcium silicates (see Figs. 3 and 4), calcite, and hydrous silica. This is significant as the hydrated calcium silicates and calcite are known to feature a mutual affinity for attachment and growth [43,49,50].

Of course, up on extended exposure to CO₂, the hydrated calcium silicates would decompose to form calcite and hydrous silica (as shown in Fig. 3), which have themselves been noted to offer cementation

¹ It should be noted that $> 65\%$ of all concretes produced globally (i.e., primarily using OPC as the cementitious reactant) feature a compressive strength of 30 MPa or less [42].

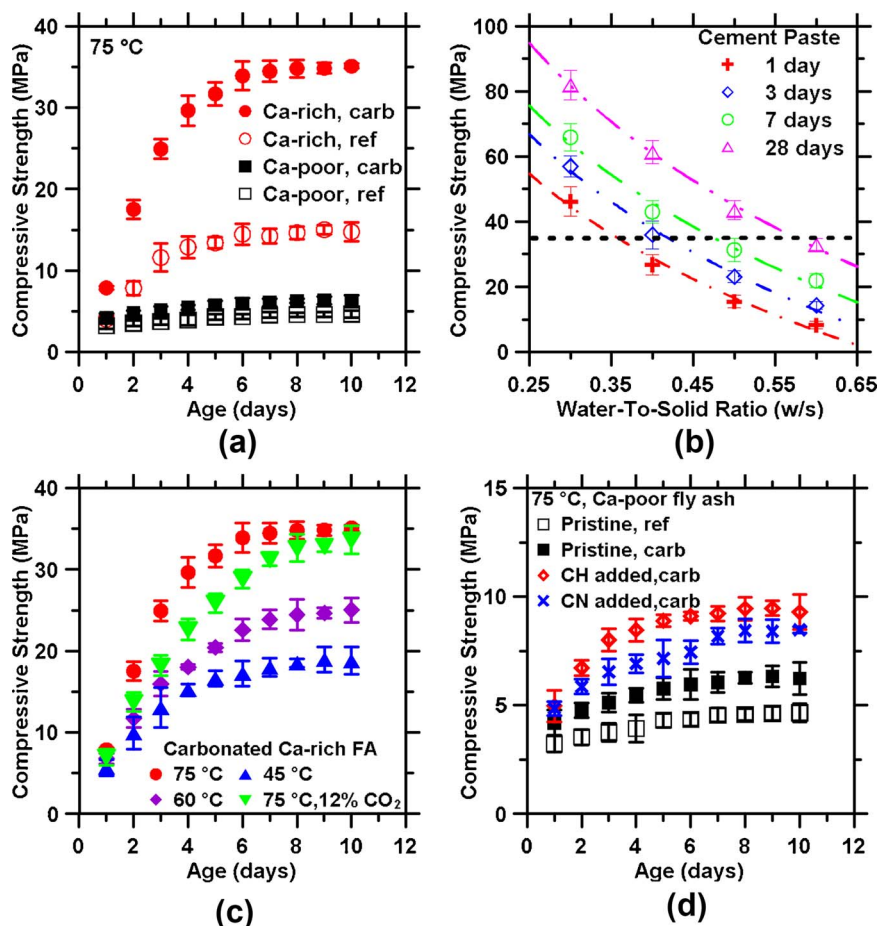


Fig. 2. The evolution of compressive strengths of: (a) Ca-rich and Ca-poor fly ash pastes following CO₂ exposure at 75 °C, and the control samples (i.e., exposed to pure N₂) for comparison, as a function of (carbonation) time, (b) hydrated OPC pastes at different ages after curing in limewater at 23 °C, as a function of w/s. The dashed black line shows the compressive strength of a Ca-rich fly ash formulation following its exposure to CO₂ at 75 °C for 7 days, (c) Ca-rich fly ash pastes carbonated at different temperatures following exposure to 99.5% CO₂ (v/v) and simulated flue gas (12% CO₂, v/v), as a function of time, and, (d) Ca-enriched (i.e., with added Ca(OH)₂ or dissolved Ca(NO₃)₂) Ca-poor (i.e., Class F) fly ash pastes following CO₂ exposure at 75 °C, as a function of time. The compressive strengths of the pristine Ca-poor fly ash with and without carbonation are also shown for comparison.

[7,51]. Similar mechanisms of carbonation strengthening have been noted following the reaction of low-rank, synthetic calcium silicates with CO₂ [52,53]. The systematic formation of mineral carbonates in this fashion induces: (i) cementation, e.g., in a manner analogous to that observed in mollusks, and sea-shells, that binds proximate particles to each other via a carbonate network, or carbonate formation which ensures the cementation of sandstones [54–58], and, (ii) an increase in the total volume of solids formed which results in a densification of microstructure, while ensuring CO₂ uptake (e.g., see Vance et al. [7] and Fig. 3 for scenarios wherein reaction with CO₂ results in an increase in solid volume).

Coming back to ascertaining the ability of flue gas from coal-fired power plants, as is, to carbonate fly ash, the Ca-rich fly ash was carbonated in a 12% CO₂ atmosphere (v/v) at 75 °C. As noted in Fig. 2(c) and Fig. 3(b, e), CO₂ present in flue gas at relevant concentrations can readily carbonate fly ash and ensure strength gain, albeit at a slightly reduced rate vis-à-vis pure CO₂ exposure. This reduced rate of strength gain (and carbonation) is on account of the lower abundance of dissolved CO₂ in the vapor phase [17], and hence in the liquid water following Henry's law [32,59]. However, it should be noted that after 10 days of exposure to simulated flue gas, the strength of the Ca-rich fly ash formulation was equivalent to those cured in a pure-CO₂ atmosphere (Fig. 2c). This is significant, as it demonstrates a pathway for clinkering-free cementation by synergistic use of both fly ash and untreated flue gas of dilute CO₂ concentrations sourced from coal-fired power plants.

To better assess the potential for valorization of diverse industrial waste streams of CO₂, the effects of reaction temperature on carbonation and strength gain were further examined. As an example, flue gas emitted from coal-fired power plants features an exit temperature (T_E) on the order of $50\text{ °C} \leq T_E \leq 140\text{ °C}$ to minimize fouling and corrosion,

and to provide a buoyant force to assist in the evacuation of flue gas through the stack [60]. Since heat secured from the flue gas is foreseen as the primary means of thermal activation of reactions, the carbonation of Ca-rich fly ash formulations and their rate of strength gain were examined across a range of temperatures as shown in Fig. 2(c). Expectedly, the rate of strength gain increases with temperature. This is on account of two factors: (i) elevated temperatures facilitate the dissolution of the fly ash solids [20], and the leaching of the fly ash glass [18,20], and, (ii) elevated temperatures favor the drying of the fly ash formulation, thereby easing the transport of CO₂ into the pore structure which facilitates carbonation [21]. It should however be noted that the solubility of CO₂ in water decreases rapidly with increasing temperature. While in a closed system this may suppress the rate of carbonation, the continuous supply of CO₂ provisioned herein, in a condensing atmosphere ensures that no retardation in carbonation kinetics is observed despite an increase in temperature. It should also be noted that the net carbonation reactions are exothermic [17]. Therefore, increasing the reaction temperature is expected to retard reaction kinetics (i.e., following Le Chatelier's principle [59]); unless heat were to be carried away from the carbonating material. Of course, such exothermic heat release would further decrease the solubility of CO₂ in water by enhancing the local temperature in the vicinity of the reaction zone. As such, several processes including the dissolution of the fly ash solids, leaching of the fly ash glass, and the transport of solubilized CO₂ through the vapor phase and water present in the pore structure influence the rate of fly ash carbonation.

To more precisely isolate the role of total Ca content of the fly ash, further experiments were carried out wherein Ca(OH)₂ or Ca(NO₃)₂ were added to the Ca-poor fly ash in order to produce bulk Ca contents equivalent to the Ca-rich fly ash. Here, it should be noted that while Ca(OH)₂ was added as a solid that was homogenized with the fly ash, Ca

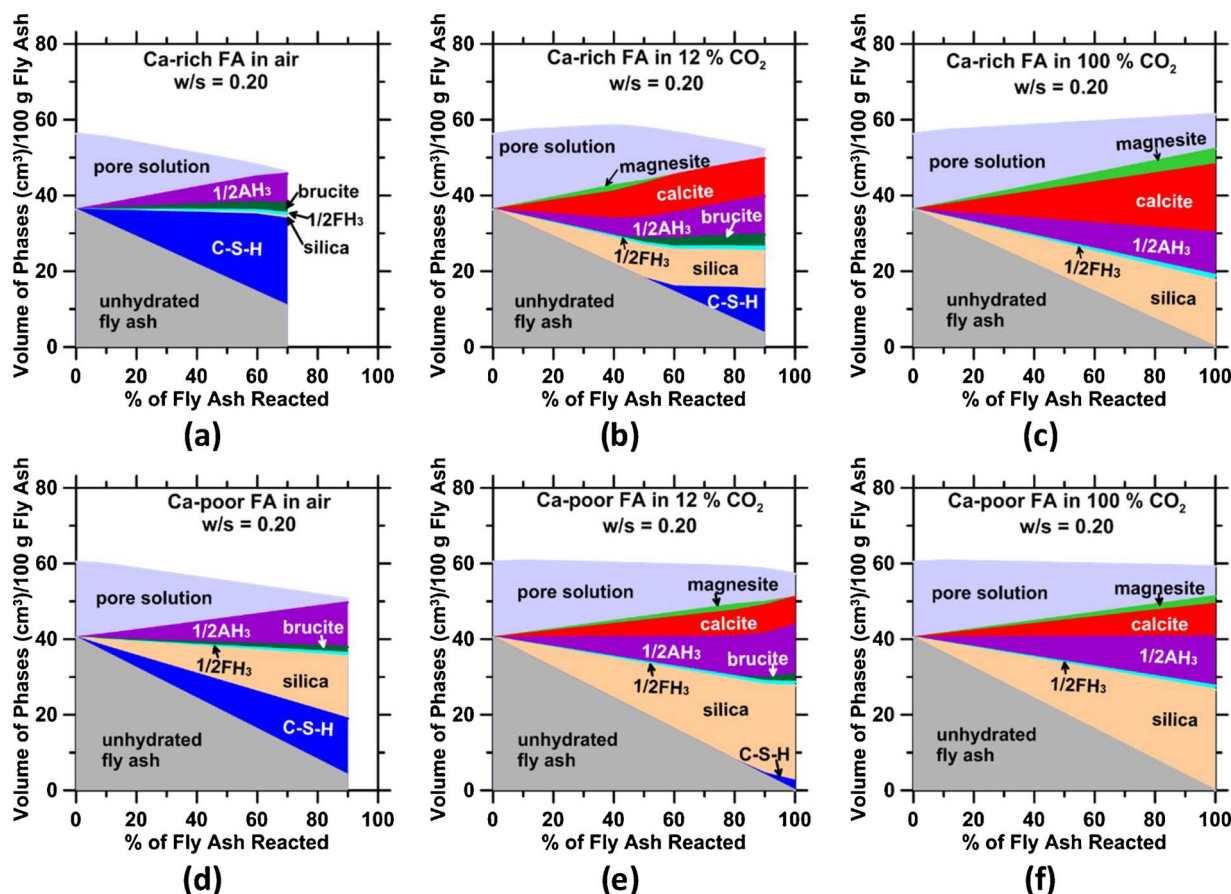


Fig. 3. The GEMS-calculated solid phase balances as a function of the extent of fly ash reaction for Ca-rich and Ca-poor fly ash in the presence of a gas-phase consisting of: (a, d) air, (b, e) 12% CO₂ (i.e., simulated flue gas environment), and (c, f) 100% CO₂ at T = 75 °C and p = 1 bar for w/s = 0.20. Here, 1/2FH₃ = Fe(OH)₃, 1/2AH₃ = Al(OH)₃, silica = hydrous silica, and C-S-H = calcium silicate hydrate. The solid phase distribution is calculated until the pore solution is exhausted, or the fly ash reactant is completely consumed.

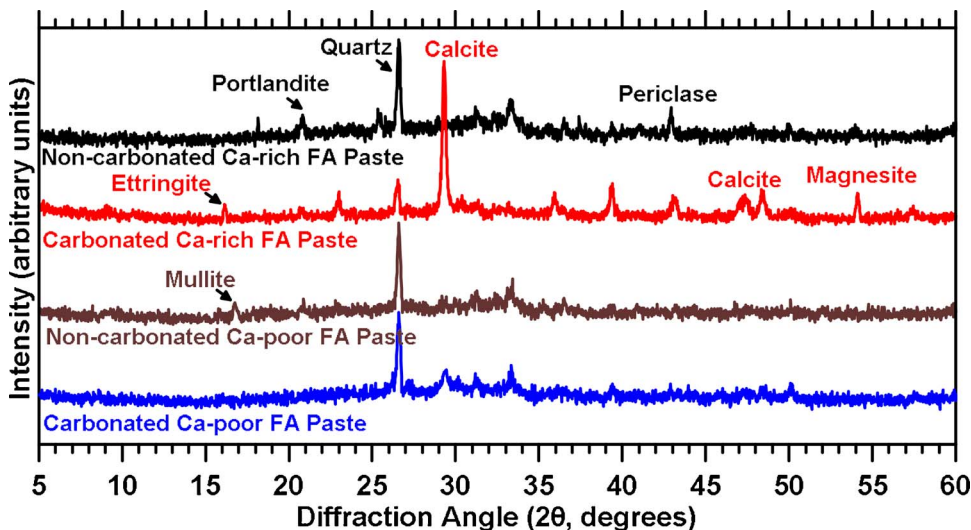


Fig. 4. Representative XRD patterns of Ca-rich and Ca-poor fly ash formulations before and after exposure to CO₂ at 75 °C for 10 days. The Ca-poor fly ash shows no change in the nature of compounds present following exposure to CO₂.

(NO₃)₂ was solubilized in the mixing water. The results shown in Fig. 2(d) highlight that although the Ca(OH)₂- and Ca(NO₃)₂-enriched Ca-poor fly ashes experienced substantial strength increases (≈ 35%) following carbonation as compared to the pristine Ca-poor fly ash, the strengths were still far lower than that of the Ca-rich fly ash (see Fig. 2a). These observations demonstrate that the presence of Ca is not a sufficient condition to assume carbonation. An example of this is CaO, which although abundant in Ca will carbonate only superficially due to kinetic restraint on the progress of carbonation reactions that is

imposed by the formation of a passivation layer of CaCO₃ on its surface [61,62]. Nevertheless, the enhancement in strength observed in the Ca-poor formulations is postulated to be on the account of both: (a) the pozzolanic reaction between the added Ca source and silica liberated from the fly ash resulting in the formation of calcium silicate hydrates (C-S-H), and, (b) the formation of calcite and (hydrous) silica gel by the carbonation-decomposition of C-S-H, and by direct reaction of solubilized Ca with aqueous carbonate species [63]. The carbonation of C-S-H has been observed to result in the release of free water and the

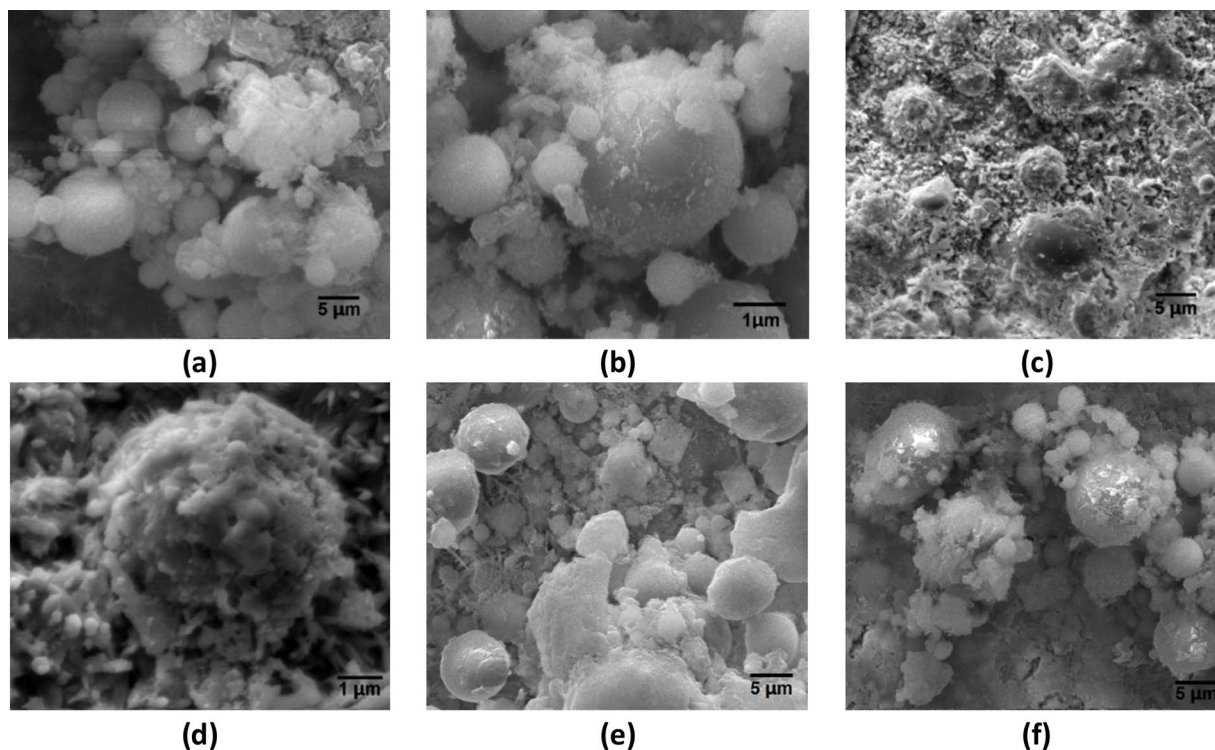


Fig. 5. Representative SEM micrographs of: (a) a Ca-rich fly ash formulation following exposure to N₂ at 75 °C for 10 days; a magnified image highlighting the surface of a fly ash particle is shown in (b), (c) a Ca-rich fly ash formulation following exposure to pure CO₂ at 75 °C for 10 days; a magnified image highlighting the surface of a carbonated fly ash particle wherein carbonation products in the form of calcite are clearly visible on the particle surface is shown in (d), (e) a Ca-poor fly ash formulation following exposure to pure CO₂ at 75 °C for 10 days, and (f) Ca(OH)₂-enriched Ca-poor fly ash formulation following exposure to pure CO₂ at 75 °C for 10 days wherein the limited formation of calcite is noted on particle surfaces.

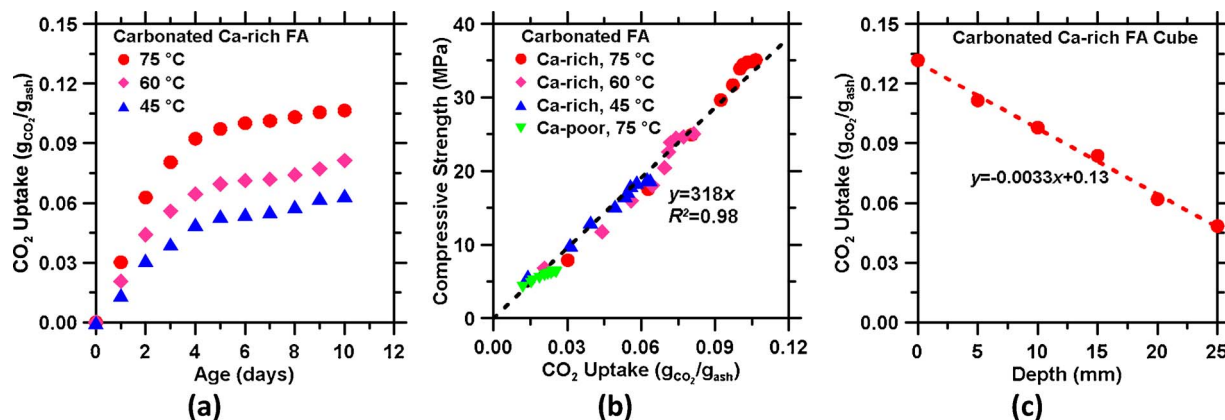


Fig. 6. (a) The CO₂ uptake (normalized by the mass of Ca-rich fly ash in the formulation) as a function of time for samples exposed to pure CO₂ at different temperatures. The amount of CO₂ uptake was estimated using the mass-based method. (b) The compressive strength of the Ca-rich and Ca-poor fly ash samples as a function of their CO₂ uptake following exposure to pure CO₂ at different temperatures for up to 10 days. The data reveals a strength gain rate of 3.2 MPa per unit mass of fly ash that has reacted (carbonated). The amount of CO₂ uptake was estimated using the mass-based method. (c) The CO₂ uptake of a Ca-rich fly ash formulation as a function of depth. The macroscopic sample consisted of a cube (50 mm × 50 mm × 50 mm) that was exposed to pure CO₂ at 75 °C for 10 days. Herein, CO₂ uptake was assessed by thermal analysis (TGA).

formation of a silica gel with reduced water content [63–65]. However, such water release (i.e., an increase in the porosity) does not appear to be the cause of the reduced strengths obtained in the Ca-poor fly ash formulations [63]. Rather, it appears as though the presence of reactive Ca intrinsic to the fly ash (glass), and the formation of a silica-rich surface layer to which CaCO₃ can robustly adhere results in higher strength development in Ca-rich fly ash formations. Given the inability of Ca-poor fly ashes to offer substantial carbonation-induced strength gain, the remainder of the study focuses on better assessing the effects of CO₂ exposure on Ca-rich fly ash formulations.

Indeed, the electron micrographs shown in Fig. 5 offer additional insights into morphology and microstructure development in Ca-rich fly ash formulations following exposure to N₂ and CO₂ at 75 °C for 10 days.

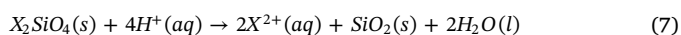
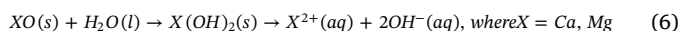
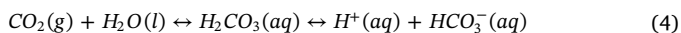
First, it is noted that the uncarbonated fly ash formulations show a loosely packed microstructure with substantial porosity (Fig. 5a). Close examination of a fly ash particle shows a “smooth” surface (e.g., see Fig. 5b), although alkaline species might have been leached from the particle’s surface. In contrast, Fig. 5(c–d) reveal the formation of a range of crystals that resemble “blocks and peanut-like aggregates” on the surfaces of Ca-rich fly ash particles – post-carbonation. XRD (Fig. 4) and SEM-EDS analyses of these structures confirm their composition as that of calcium carbonate (calcite: CaCO₃). These observations are in agreement with those of Fernandez-Diaz et al. [66] and Vance et al. [7], who reported such altered morphologies of calcite crystals. Nevertheless, the role of calcite and silica gel that forms in these systems is significant in that such solids serve to reduce the

porosity [67], and effectively bind the otherwise loosely packed fly ash particles (Fig. 5a), thereby ensuring “carbonation strengthening”. Expectedly, Ca-poor fly ash particles do not show the formation of carbonation products on their surfaces, in spite of CO₂ exposure (see Fig. 5e). Furthermore, the addition of supplemental portlandite to Ca-poor systems results in only a marginal level of carbonation product formation on fly ash particle surfaces (see Fig. 5f). These observations highlight the critical role of not only the Ca (and Mg)-content, but also potentially their spatial distribution on microstructure and strength development in carbonated fly ash systems.

3.2. Carbonation kinetics

Fig. 6(a) shows CO₂ uptake by the Ca-rich fly ash formulation as determined by thermal analysis (i.e., by tracking the decomposition of CaCO₃) as a function of time across a range of curing temperatures. For the conditions relevant to this study, both the rate and extent of CO₂ uptake, at a given time, increase with temperature. Although the terminal CO₂ uptake (i.e., which is a function of chemical composition) is expected to be similar across all conditions, this was not observed over the course of these experiments—likely due to kinetic limitations on dissolution, and the subsequent carbonation of the fly ash solids. Nevertheless, a linear correlation between compressive strength evolution and the CO₂ uptake of a given mixture is noted (see Fig. 6b)—for both Ca-rich and Ca-poor fly ash formulations. Significantly, a strength gain on the order of 3.2 MPa per unit mass of fly ash carbonated is realized. It should be noted that the Ca-rich fly ash composition examined herein—in theory—has the potential to take-up around 27.1 mass% CO₂ assuming that all the CaO and MgO therein would carbonate (e.g., see XRF composition in Table 1). Based on the correlation noted in Fig. 6(b), realizing the highest possible maximum carbonation level—i.e., at thermodynamic equilibrium would produce a terminal strength on the order of 86 MPa independent of the prevailing reaction conditions (i.e., CO₂ concentration, and temperature). It should be noted however that achieving this terminal level of CO₂ uptake is unlikely due to the time-dependent: (i) formation of carbonate films of increasing thickness which hinders access to the reactants [7], and, (ii) formation of a dense microstructure that hinders the transport of CO₂ through the liquid phase to reactive sites.

Broadly, mineral carbonation, i.e., the formation of calcite and/or magnesite, takes the form of irreversible heterogeneous solid-liquid-gas reactions [68–73]. In the case of Ca-rich fly ashes, it includes the processes of dissolution and hydration of the Ca-rich compounds including Ca-silicates, Ca-rich glasses, CaO, Ca(OH)₂, etc., and the subsequent precipitation of CaCO₃ from aqueous solution; e.g., see Table 2, Fig. 3, and the following reactions:



Simultaneous to the dissolution and hydration of the solids, vapor phase CO₂ will dissolve in water, as dictated by its equilibrium solubility at the relevant pH and temperature [74]. As ionized species from the reactants and dissolved CO₂ accumulate in the liquid phase, up on achieving supersaturation—often described by the ratio of the ion activity product to the solubility product for a given compound, e.g., calcite [59]—precipitation occurs thereby reducing the supersaturation level. Ca- or Mg-bearing compounds in the fly ash would continue to dissolve as the solution remains undersaturated with respect to these phases due to the precipitation of carbonates, ensuring the formation of Ca- and Mg-carbonates until the readily available quantity of these

reactant compounds is exhausted and the system reaches equilibrium. It should be noted that a high pH is expected to be maintained in the pore solution because of the abundance of alkaline compounds in the fly ash mixture.

It should furthermore be noted that, in the case of the fly ash cubes tested for compressive strength (i.e., following ASTM C109 [31]) (see Fig. 6c, and associated thin-section analysis; not shown) or in the case of fly ash particulates (e.g., see Fig. 5), in general, carbonation reactions proceed inward from the surface to the interior and the surface reacts faster than the bulk [18,74,75]. The kinetics of such reactions can be analyzed by assessing how the rate of conversion of the reactants is affected by process variables [76]. For example, as noted above in Fig. 6(a), it is seen that carbonation occurs rapidly at short reaction times, and its rate progressively decreases with increasing reaction time. This nature of rapid early-reaction, followed by an asymptotic reduction in the reaction rate at later times has been previously attributed to: (i) the nucleation and growth of carbonate crystals which occurs at early reaction times, and whose rate of formation is a function of the surface area of the reactant [68,72], and, (ii) a diffusion-(transport-) limited process which requires CO₂ species to transport to microstructure hindered sites wherein carbonation occurs [7,17,22,23,74]. Such kinetics can be described by a generalized reaction-diffusion model as shown in Eq. (9) [21]:

$$[1 - (1 - \alpha)^{\frac{1}{3}}]^n = kt \quad (9)$$

where, α is the CO₂ uptake ratio (g of CO₂ uptake per g of reactant, i.e., fly ash), t is the time (days, d), k (d⁻¹) is the apparent reaction rate constant, and n is an index related to the rate-determining step. For example, $n = 1$ represents the commonly used “contracting volume model” for rapid initial nucleation and growth of products from the reactants from an outer surface of a spherical shape [21,69,71,72]. When $n = 2$, Eq. (9) reduces to Jander’s model for diffusion-controlled reactions [22,69,71,72], wherein the reaction rate is determined by the transport of reactants through the product layer to the reaction interface. It should be noted that herein, the presence of liquid water serves to catalyze carbonation reactions, by offering a high pH medium that can host mobile CO₃²⁻ ions [7].

Fig. 7(a) shows fits of Eq. (9) to the experimental carbonation data taken from Fig. 6(a) for different carbonation temperatures. A clear change in slope is noted just prior to a reaction interval of 2 days. Across all temperatures, initially the slopes (m, unitless) of all the curves, wherein $m = 1/n$, are on the order of: $m = 1 \pm 0.2$, while after 2 days, $m = 0.5 \pm 0.1$. The slight deviation of the slopes from their ideal values ($n = 1$ and 2) is postulated to be on account of the wide-size distributions of the fly ash particles and the irregular coverage of particles offered by the carbonation products, e.g., as shown in Fig. 5. And indeed, typical reaction models were developed assuming monodisperse, spherical reactant particles [72,76]. The rate constants obtained from the fittings shown in Fig. 7(a) were used to calculate the apparent activation energy of the two steps of carbonation reactions, i.e., a topochemical reaction step, followed by a diffusion-limited step as shown in Fig. 7(b). This analysis reveals: (i) $E_{a,1} = 8.9$ kJ/mol for surface nucleation reactions indicative of a small dependence of reaction rate on temperature, similar to that observed by Vance et al. for the carbonation of portlandite [7], and, (ii) $E_{a,2} = 24.1$ kJ/mol for diffusion-controlled reaction; a value similar to that observed by Fernandez et al. [77], and Sun et al. [21] for the carbonation of MgO, and CaO respectively. The fact that the activation energy for surface nucleation reaction is much lower than that for diffusion-controlled reaction suggests that the carbonation reaction is dominated by nucleation and growth of carbonation products initially. However, as carbonation reaction progresses, the precipitation of carbonation products results in the formation of a barrier layer on the fly ash particles (see Fig. 5)—that binds the particles together and simultaneously increases the resistance to the transport of CO₂ species to carbonation sites. As a result, the

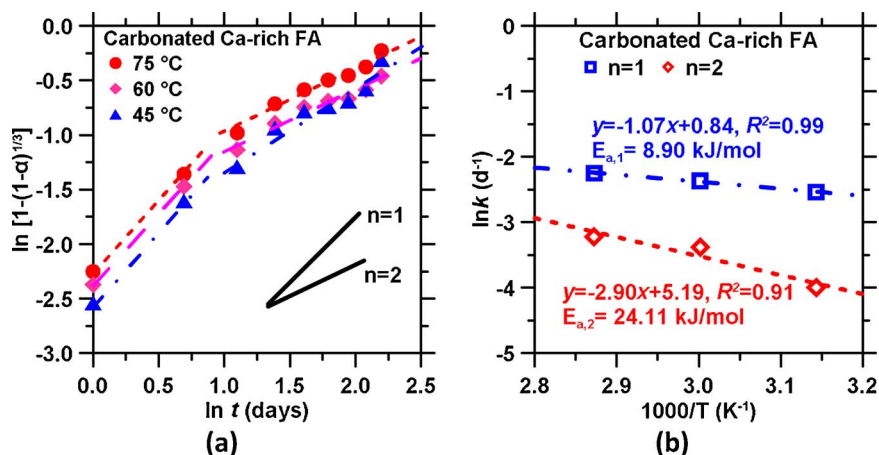


Fig. 7. (a) Kinetic analysis of carbonation reactions occurring in Ca-rich fly ash formulations reacting at different temperatures in pure CO₂ over a period of 10 days. The data were fitted using the (surface) reaction-diffusion model shown in Eq. (9), and, (b) An Arrhenius diagram for determining the apparent activation energies of: (i) surface nucleation and growth ($n = 1$), and, (ii) diffusion of reactant species through a surficial layer ($n = 2$).

transport step assumes rate control in the later stages of carbonation reactions [19,21].

4. Summary and conclusions

This paper has demonstrated an original means for clinkering-free cementation by fly ash carbonation. Specifically, it is shown that Ca-rich fly ashes that host substantial quantities of Ca (and Mg) in the form of crystalline compounds, or in the glassy phases readily react with dilute concentrations of CO₂ in moist environments, at ambient pressure, and at sub-boiling temperatures to produce cemented solids whose properties are sufficient for use in structural construction. Indeed, Ca-rich fly ash solids, following CO₂ exposure achieve a strength of around 35 MPa after 7 days, and take-up 9% CO₂ by mass of reactant solids. Detailed results from thermodynamic modeling, XRD analyses, and SEM observations suggest that fly ash carbonation results in the formation of a range of reaction products, namely calcite, hydrous silica, and potentially some C-S-H which collectively bond proximate particles into a cemented solid. Careful analysis of kinetic (rate) data using a reaction-diffusion model highlights two rate-controlling reaction steps: (a) where the surface area of the reactants, and the nucleation and growth of carbonate crystals there upon is dominant at early reaction times ($E_{a,1} = 8.9$ kJ/mol), and, (b) a later-age process which involves the diffusion of CO₂ species through thickening surficial barriers on reactant sites ($E_{a,2} = 24.1$ kJ/mol). It is noted that due to their reduced content of accessible Ca and Mg species, Ca-poor fly ashes feature limited potential vis-à-vis Ca-rich fly ashes for CO₂ uptake, and carbonation strengthening. Although the provision of extrinsic Ca sources to Ca-poor fly ashes can somewhat offset this lack, our observations suggest that not only the total amount (mass abundance) of Ca and Mg, but also its reactivity and spatial distribution are all important in determining a fly ash solid's suitability for CO₂ uptake, and in turn, carbonation strengthening. Furthermore, it is noted that strength gain is linearly related to the extent of carbonation (CO₂ uptake). This suggests a straightforward means to estimate strength gain if the extent of carbonation may be known, or vice-versa. These observations are significant in that they demonstrate a new route for producing cemented solids by an innovative clinkering-free, carbonation based pathway.

5. Implications on solid and flue gas CO₂ waste valorization in coal-fired power plants

Electricity generation from coal and natural gas combustion results in the production of substantial quantities of combustion residues and CO₂ emissions. For example, in the United States alone, coal combustion (for electricity production) resulted in the production of nearly 120 million tons of coal-combustion residuals (CCRs) [78,79], and 1.2 billion tons of CO₂ emissions in 2016 [80]. While some CCRs find use in

other industries (e.g., flue gas desulfurization (FGD) gypsum, fly ash, etc.), the majority of CCRs continue to be land-filled. For example, in the U.S., only around 45% of the annual production of fly ash is beneficially utilized—e.g., to replace cement in the binder fraction in traditional concrete—while the rest is disposed in landfills [11,79]. Such underutilization stems from the presence of impurities in the fly ash including unburnt carbon and calcium sulfate that forms due to the sulfation of lime that is injected for air pollution control (APC) [13,15], compromising the durability of traditional concrete. The materials examined herein, i.e., fly ashes that are cemented by carbonation, are not expected to be affected by the presence of such impurities—as a result, a wide range of Ca-rich fly ash sources—including those containing impurities, and mined from historical reservoirs (i.e., “ash ponds”) are expected to be usable for carbonation-based fly ash cementation. When coupled with the fact that fly ash carbonation can be effected at sub-boiling temperatures using dilute, untreated (flue-gas) CO₂ streams, the outcomes of this work create a pathway for the simultaneous utilization of both solid- and vapor-borne wastes created during coal combustion. Such routes for waste, and especially CO₂ valorization create value-addition pathways that can be achieved without a need for carbon capture (i.e., or more correctly CO₂ concentration enhancement), thereby offering a line-of-sight to economic viability in commercial markets [81] (N.B.: Based on current best-available technologies (BATs), CO₂ capture using an amine stripper is expected to induce a financial burden of \$ 60-to-90 per ton of CO₂ in addition to inducing parasitic energy losses for solvent regeneration [82,83]). Importantly, the simplicity of this carbonation process ensures that it well-suited for co-location (“bolt-on, stack-tap” integration) with large point-source CO₂ emission sites including petrochemical facilities, coal/natural gas fired power plants, and cement plants. In each case, emitted flue gas can be used to provide both waste heat to hasten chemical reactions, and CO₂ to ensure mineralization without imposing any additional needs for emissions control. The proposed approach is significant since—within a traditional lifecycle analysis (LCA) framework wherein there is no embodied CO₂ impact associated with reactants such as coal combustion wastes or emitted CO₂, and wherein processing energy (heat) is secured from the flue gas stream—fly ash carbonation, by virtue of active CO₂ uptake, and CO₂ avoidance (i.e., by diminishing the production and use of OPC) has the potential to yield CO₂ negative pathways for cementation, and hence construction. New approaches of this nature are critical to create commercially viable routes for CO₂ utilization, and thereby accelerate the development and maturation of a viable carbon-to-value (CTV) economy [84].

Acknowledgements

The authors acknowledge financial support for this research from the: Department of Energy, Office of Fossil Energy via the National

Energy Technology Laboratory (NETL; DE-FE0029825), Anthony and Jeanne Pritzker Foundation, and the National Science Foundation (CAREER Award: 1235269). This research was conducted in the Laboratory for the Chemistry of Construction Materials (LC²), Molecular Instrumentation Center (MIC), and the Electron Microscopy Core Facility at UCLA. As such, the authors gratefully acknowledge the support that has made these laboratories and their operations possible. The contents of this paper reflect the views and opinions of the authors, who are responsible for the accuracy of the datasets presented herein, and do not reflect the views and/or policies of the funding agencies, nor do the contents constitute a specification, standard or regulation.

References

- J.J. Biernacki, J.W. Bullard, G. Sant, K. Brown, F.P. Glasser, S. Jones, T. Ley, R. Livingston, L. Nicoleau, J. Olek, F. Sanchez, R. Shahsavari, P.E. Stutzman, K. Sobolev, T. Prater, Cements in the 21st century: challenges, perspectives, and opportunities, *J. Am. Ceram. Soc.* 100 (2017) 2746–2773.
- C. Shi, A.F. Jiménez, A. Palomo, New cements for the 21st century: the pursuit of an alternative to Portland cement, *Cem. Concr. Res.* 41 (2011) 750–763.
- M. Schneider, M. Romer, M. Tschudin, H. Bolio, Sustainable cement production—present and future, *Cem. Concr. Res.* 41 (2011) 642–650.
- Mineral Commodity Summaries, U.S. Geological Survey, (2017) <https://minerals.usgs.gov/minerals/pubs/mcs/2017/mcs2017.pdf> (Accessed 18 September 2017).
- P.K. Mehta, P.J.M. Monteiro, *Concrete: Microstructure, Properties, and Materials*, fourth edition, McGraw-Hill, 2014.
- S. Mindess, J.F. Young, D. Darwin, *Concrete*, second edition, Prentice Hall, 2003.
- K. Vance, G. Falzone, I. Pignatelli, M. Bauchy, M. Balonis, G. Sant, Direct carbonation of Ca(OH)₂ using liquid and supercritical CO₂: implications for carbon-neutral cementation, *Ind. Eng. Chem. Res.* 54 (2015) 8908–8918.
- T. Hemalatha, A. Ramaswamy, A review on fly ash characteristics—towards promoting high volume utilization in developing sustainable concrete, *J. Clean. Prod.* 147 (2017) 546–559.
- Trends in Global CO₂ Emissions, 2016 Report, PBL Netherlands Environmental Assessment Agency, 2017 http://edgar.jrc.ec.europa.eu/news_docs/jrc-2016-trends-in-global-co2-emissions-2016-report-103425.pdf (Accessed 1 June 2017).
- G. Montes-Hernandez, R. Perez-Lopez, F. Renard, J.M. Nieto, L. Charlet, Mineral sequestration of CO₂ by aqueous carbonation of coal combustion fly-ash, *J. Hazard. Mater.* 161 (2009) 1347–1354.
- J. Vargas, A. Halog, Effective carbon emission reductions from using upgraded fly ash in the cement industry, *J. Clean. Prod.* 103 (2015) 948–959.
- Coal Combustion Residual Beneficial Use Evaluation: Fly Ash Concrete and FGD Gypsum Wallboard, U.S. Environmental Protection Agency, 2017 February https://www.epa.gov/sites/production/files/2014-12/documents/ccr_bu_app.pdf (Accessed 1 June 2017).
- ASTM International, ASTM Standard C618: Standard Specification for Coal Fly Ash and Raw or Calcined Natural Pozzolan for Use in Concrete, ASTM International, West Conshohocken, PA, 2015.
- S.H. Kosmatka, B. Kerkhoff, W.C. Panarese, *Design and Control of Concrete Mixtures*, Portland Cement Association, 2002.
- M. Ahmaruzzaman, A review on the utilization of fly ash, *Prog. Energy Combust. Sci.* 36 (2010) 327–363.
- S. Kumar, R. Kumar, A. Bandopadhyay, Innovative methodologies for the utilisation of wastes from metallurgical and allied industries, *Resour. Conserv. Recycl.* 48 (2006) 301–314.
- A. Sanna, M. Uibu, G. Caramanna, R. Kuusk, M.M. Maroto-Valer, A review of mineral carbonation technologies to sequester CO₂, *Chem. Soc. Rev.* 43 (2014) 8049–8080.
- J. Jaschik, M. Jaschik, K. Warmuziński, The utilisation of fly ash in CO₂ mineral carbonation, *Chem. Process Eng.* 37 (2016) 29–39.
- V. Romanov, Y. Soong, C. Carney, G.E. Rush, B. Nielsen, W. O'Connor, Mineralization of carbon dioxide: a literature review, *ChemBioEng. Rev.* 2 (2015) 231–256.
- N.L. Ukwattage, P.G. Ranjith, M. Yellishetty, H.H. Bui, T. Xu, A laboratory-scale study of the aqueous mineral carbonation of coal fly ash for CO₂ sequestration, *J. Clean. Prod.* 103 (2015) 665–674.
- J. Sun, M.F. Bertos, S.J.R. Simons, Kinetic study of accelerated carbonation of municipal solid waste incinerator air pollution control residues for sequestration of flue gas CO₂, *Energy Environ. Sci.* 1 (2008) 370.
- S. Tian, J. Jiang, X. Chen, F. Yan, K. Li, Direct gas-solid carbonation kinetics of steel slag and the contribution to in situ sequestration of flue gas CO₂ in steel-making plants, *ChemSusChem* 6 (2013) 2348–2355.
- S. Tian, J. Jiang, K. Li, F. Yan, X. Chen, Performance of steel slag in carbonation–calcination looping for CO₂ capture from industrial flue gas, *RSC Adv.* 4 (2014) 6858–6862.
- M.G. Nyambura, G.W. Mugeru, P.L. Felicia, N.P. Gathura, Carbonation of brine impacted fractionated coal fly ash: implications for CO₂ sequestration, *J. Environ. Manage.* 92 (2011) 655–664.
- W. Ashraf, Carbonation of cement-based materials: challenges and opportunities, *Constr. Build. Mater.* 120 (2016) 558–570.
- ASTM International, ASTM Standard C150/C150M: Standard Specification of Portland Cement, ASTM International, 2012 West Conshohocken, PA.
- T. Oey, J. Timmons, P. Stutzman, J.W. Bullard, M. Balonis, M. Bauchy, G. Sant, An improved basis for characterizing the suitability of fly ash as a cement replacement agent, *J. Am. Ceram. Soc.* 00 (2017) 1–16.
- Z. Wei, G. Falzone, B. Wang, A. Thiele, G. Puerta-Falla, L. Pilon, N. Neithalath, G. Sant, The durability of cementitious composites containing microencapsulated phase change materials, *Cem. Concr. Compos.* 81 (2017) 66–76.
- ASTM International, ASTM Standard C192/C192M: Standard Practice for Making and Curing Concrete Test Specimens in the Laboratory, ASTM International, West Conshohocken, PA, 2012.
- IPCC, 2014: Climate Change 2014: Synthesis Report. Contribution of Working Groups I, II and III to the Fifth Assessment Report of the Intergovernmental Panel on Climate Change [Core Writing Team, R.K. Pachauri and L.A. Meyer (eds.)]. IPCC, Geneva, Switzerland, 151 pp.
- ASTM International, ASTM Standard C109/C109M: Standard Test Method for Compressive Strength of Hydraulic Cement Mortars, ASTM International, West Conshohocken, PA, 2012.
- J.J. Carroll, J.D. Slupsky, A.E. Mather, The solubility of carbon dioxide in water at low pressure, *J. Phys. Chem. Ref. Data* 20 (1991) 1201–1209.
- D. Kulik, U. Berner, E. Curti, Modelling chemical equilibrium partitioning with the GEMS-PSI code, PSI Scientific Report, (2004).
- D. Kulik, T. Wagner, S. Dmytrieva, G. Kosakowski, F. Hingerl, K. Chudnenko, U. Berner, GEM-Selektor geochemical modeling package: revised algorithm and GEMS3K numerical kernel for coupled simulation codes, *Comput. Geosci.* 17 (2013) 1–24.
- T. Thoenen, D. Kulik, Nagra/PSI Chemical Thermodynamics Database 01/01 for the GEM-Selektor (V.2-PSI) Geochemical Modeling Code, (2003) PSI TM-44-02-09.
- J.W. Johnson, E.H. Oelkers, H.C. Helgeson, SUPCRT92. A software package for calculating the standard molal thermodynamic properties of minerals, gases, aqueous species, and reactions from 1 to 5000 bar and 0 to 1000 °C, *Comput. Geosci.* 18 (1992) 899–947.
- W. Hummel, U. Berner, E. Curti, F. Pearson, T. Thoenen, Nagra/PSI Chemical Thermodynamic Database 01/01, Also Published as Nagra Technical Report NTB 02-16, (2002) Wettingen, Switzerland.
- B. Lothenbach, T. Matschei, G. Moschner, F.P. Glasser, Thermodynamic modelling of the effect of temperature on the hydration and porosity of Portland cement, *Cem. Concr. Res.* 38 (2008) 1–18.
- T. Matschei, B. Lothenbach, F.P. Glasser, Thermodynamic properties of Portland cement hydrates in the system CaO–Al₂O₃–SiO₂–CaSO₄–CaCO₃–H₂O, *Cem. Concr. Res.* 37 (2007) 1379–1410.
- B. Lothenbach, F. Winnefeld, Thermodynamic modelling of the hydration of Portland cement, *Cem. Concr. Res.* 36 (2006) 209–226.
- A.H. Truesdell, B.F. Jones, WATEQ, a computer program for calculating chemical equilibria of natural waters, *J. Res. US Geol. Surv.* 2 (2) (1974) 233–248.
- Ready Mixed Concrete Industry Statistics, European Ready Mixed Concrete Organization, 2015.
- ACI Standard 318: Building Code Requirements for Structural Concrete, (2014) Farmington Hills, MI.
- A. Kumar, T. Oey, G. Falzone, J. Huang, M. Bauchy, M. Balonis, N. Neithalath, J. Bullard, G. Sant, The filler effect: the influence of filler content and type on the hydration rate of tricalcium silicate, *J. Am. Ceram. Soc.* 100 (2017) 3316–3328.
- D. Zhang, X.H. Cai, Y.X. Shao, Carbonation curing of precast fly ash concrete, *J. Mater. Civ. Eng.* 28 (2016).
- A. Mikuni, R. Komatsu, K. Ikeda, Dissolution properties of some fly ash fillers applying to geopolymeric materials in alkali solution, *J. Mater. Sci.* 42 (2007) 2953–2957.
- J.P. Hamilton, C.G. Pantano, Effects of glass structure on the corrosion behavior of sodium-aluminosilicate glasses, *J. Non-Cryst. Solids* 222 (1997) 167–174.
- F. Bouville, A.R. Studart, Geologically-inspired strong bulk ceramics made with water at room temperature, *Nat. Commun.* 8 (2017) 14655.
- T. Oey, A. Kumar, J.W. Bullard, N. Neithalath, G. Sant, The filler effect: the influence of filler content and surface area on cementitious reaction rates, *J. Am. Ceram. Soc.* 96 (2013) 1978–1990.
- F. Bellmann, G.W. Scherer, Analysis of C-S-H growth rates in supersaturated conditions, *Cem. Concr. Res.* (2017), <http://dx.doi.org/10.1016/j.cemconres.2017.1005.1007>.
- T. Wang, H. Huang, X.T. Hu, M.X. Fang, Z.Y. Luo, R.N. Guo, Accelerated mineral carbonation curing of cement paste for CO₂ sequestration and enhanced properties of blended calcium silicate, *Chem. Eng. J.* 323 (2017) 320–329.
- D. Daval, I. Martinez, J. Corvisier, N. Findling, B. Goffe, F. Guyot, Carbonation of Ca-bearing silicates, the case of wollastonite: experimental investigations and kinetic modeling, *Chem. Geol.* 265 (2009) 63–78.
- W.J.J. Huijgen, G.J. Witkamp, R.N.J. Comans, Mechanisms of aqueous wollastonite carbonation as a possible CO₂ sequestration process, *Chem. Eng. Sci.* 61 (2006) 4242–4251.
- F. Barthelet, H. Tang, P.D. Zavattieri, C.M. Li, H.D. Espinosa, On the mechanics of mother-of-pearl: a key feature in the material hierarchical structure, *J. Mech. Phys. Solids* 55 (2007) 306–337.
- H.L. Gao, S.M. Chen, L.B. Mao, Z.Q. Song, H.B. Yao, H. Colfen, X.S. Luo, F. Zhang, Z. Pan, Y.F. Meng, Y. Ni, S.H. Yu, Mass production of bulk artificial nacre with excellent mechanical properties, *Nat. Commun.* 8 (2017) 287.
- U.G.K. Wegst, H. Bai, E. Saiz, A.P. Tomsia, R.O. Ritchie, Bioinspired structural materials, *Nat. Mater.* 14 (2015) 23–36.
- C. Ortiz, M.C. Boyce, Bioinspired structural materials, *Science* 319 (2008) 1053–1054.
- H.A. Lowenstam, S. Weiner, *On Biomineralization*, Oxford University Press, 1989.

- [59] P. Atkins, J. de Paula, *Elements of Physical Chemistry*, 5th ed., Oxford University Press, 2007.
- [60] S.C. Ma, J. Chai, K.L. Jiao, L. Ma, S.J. Zhu, K. Wu, Environmental influence and countermeasures for high humidity flue gas discharging from power plants, *Renew. Sustain. Energy Rev.* 73 (2017) 225–235.
- [61] H. Gupta, L.-S. Fan, Carbonation-calcination cycle using high reactivity calcium oxide for carbon dioxide separation from flue gas, *Ind. Eng. Chem. Res.* 41 (2002) 4035–4042.
- [62] V. Nikulshina, M.E. Gálvez, A. Steinfeld, Kinetic analysis of the carbonation reactions for the capture of CO₂ from air via the Ca(OH)₂-CaCO₃-CaO solar thermochemical cycle, *Chem. Eng. J.* 129 (2007) 75–83.
- [63] A. Morandeau, M. Thiery, P. Dangla, Investigation of the carbonation mechanism of CH and C-S-H in terms of kinetics, microstructure changes and moisture properties, *Cem. Concr. Res.* 56 (2014) 153–170.
- [64] T.A. Bier, J. Kropp, H.K. Hilsdorf, Carbonation and realcalinisation of concrete and hydrated cement paste, in: J.C. Maso (Ed.), *Durability of Construction Materials*, Chapman and Hall, London-New York, 1987, pp. 927–934.
- [65] T.A. Bier, J. Kropp, H.K. Hilsdorf, Form Ation of Silica Gel During Carbonation of Cementitious Systems Containing Slag Cements 14–69 *ACI Special Publications SP*, 1989, pp. 1413–1428.
- [66] L. Fernandez-Diaz, J.M. Astilleros, C.M. Pina, The morphology of calcite crystals grown in a porous medium doped with divalent cations, *Chem. Geol.* 225 (2006) 314–321.
- [67] Exploring the Chemical Properties and Performance Results of Sustainable Solidia Cement™ and Solidia Concrete™, Solidia Technologies, 2017 <https://solidiatech.com/wp-content/uploads/2014/02/Solidia-Concrete-White-Paper-FINAL-2-19-14.pdf> (Accessed 22 July 2017).
- [68] L.A. Perez-Maqueda, J.M. Criado, P.E. Sanchez-Jimenez, Combined kinetic analysis of solid-state reactions: a powerful tool for the simultaneous determination of kinetic parameters and the kinetic model without previous assumptions on reaction mechanism, *J. Phys. Chem. A* 110 (2006) 12456–12462.
- [69] F.J. Gotor, J.M. Criado, J. Malek, N. Koga, Kinetic analysis of solid-state reactions: the universality of master plots for analyzing isothermal and nonisothermal experiments, *J. Phys. Chem. A* 104 (2000) 10777–10782.
- [70] S. Vyazovkin, C.A. Wight, Isothermal and nonisothermal reaction kinetics in solids: in search of ways toward consensus, *J. Phys. Chem. A* 101 (1997) 8279–8284.
- [71] J.H. Sharp, G.W. Brindley, B.N. Narahari Achar, Numerical data for some commonly used solid state reaction equations, *J. Am. Ceram. Soc.* 49 (1966) 379–382.
- [72] A. Khawam, R. Flanagan, Solid-state kinetic models: basics and mathematical fundamentals, *J. Phys. Chem. B* 110 (2006) 17315–17328.
- [73] Y. Sun, F. Bai, X. Lü, C. Jia, Q. Wang, M. Guo, Q. Li, W. Guo, Kinetic study of Huadian oil shale combustion using a multi-stage parallel reaction model, *Energy* 82 (2015) 705–713.
- [74] S.Y. Pan, E.E. Chang, P.C. Chiang, CO₂ capture by accelerated carbonation of alkaline wastes: a review on its principles and applications, *Aerosol Air Qual. Res.* 12 (2012) 770–791.
- [75] M. Thiery, G. Villain, P. Dangla, G. Platret, Investigation of the carbonation front shape on cementitious materials: effects of the chemical kinetics, *Cem. Concr. Res.* 37 (2007) 1047–1058.
- [76] O. Levenspiel, *Chemical Reaction Engineering*, John Wiley & Sons, New York, 1999.
- [77] A.I. Fernandez, J.M. Chimenos, M. Segarra, M.A. Fernandez, F. Espiell, Kinetic study of carbonation of MgO slurries, *Hydrometallurgy* 53 (1999) 155–167.
- [78] *Production and Use of Coal Combustion Products in the U.S.*, American Road and Transportation Builders Association, 2015.
- [79] Coal Ash Recycling Reaches 52 Percent as Production and Use Trends Shift, American Coal Ash Association, October, 2016 <https://www.aaa-usa.org/Portals/9/Files/PDFs/News-Release-Coal-Ash-Production-and-Use-2015.pdf> (Accessed 18 September 2017).
- [80] U.S. Energy Information Administration, How Much of U.S. Carbon Dioxide Emissions Are Associated with Electricity Generation? (2017) <https://www.eia.gov/tools/faqs/faq.php?id=77&t=11> (Accessed 5 September 2017).
- [81] J.M. Matter, M. Stute, S.O. Snaebjornsdottir, E.H. Oelkers, S.R. Gislason, E.S. Aradottir, B. Sigfusson, I. Gunnarsson, H. Sigurdardottir, E. Gunnlaugsson, G. Axelsson, H.A. Alfredsson, D. Wolff-Boenisch, K. Mesfin, D.F.D. Taya, J. Hall, K. Dideriksen, W.S. Broecker, Rapid carbon mineralization for permanent disposal of anthropogenic carbon dioxide emissions, *Science* 352 (2016) 1312–1314.
- [82] R.F. Service, Cost of carbon capture drops, but does anyone want it? *Science* 354 (2016) 1362–1363.
- [83] Carbon Capture, Utilization, and Storage: Climate Change, Economic Competitiveness, and Energy Security, U.S. Department of Energy, 2016 https://energy.gov/sites/prod/files/2016/09/f33/DOE%20-%20Carbon%20Capture%20Utilization%20and%20Storage_2016-09-07.pdf (Accessed 5 September 2017).
- [84] W.M. Budzianowski, Implementing carbon capture, utilisation and storage in the circular economy, *Int. J. Glob. Warm.* 12 (2017) 272–296.